Published in final edited form as:
Am J Cardiol. 2012 December 15; 110(12): 1820–1827. doi:10.1016/j.amjcard.2012.08.018.

Relation of Cytosolic Iron Excess to the Cardiomyopathy of Friedreich's Ataxia

R. Liane Ramirez, MS[a], **Jiang Qian, MD, PhD**[b], **Paolo Santambrogio, PhD**[d], **Sonia Levi, PhD**[d], and **Arnulf H. Koeppen, MD**[a,b,c]

[a]VA Medical Center, Albany, New York

[b]Department of Pathology Albany Medical College, Albany, New York

[c]Department of Neurology, Albany Medical College, Albany, New York

[d]Division of Neuroscience, San Raffaele Scientific Institute, Milan, Italy

Abstract

Cardiomyopathy is the leading cause of death in Friedreich's ataxia (FA). This autosomal recessive disease is caused by a homozygous guanine-adenine-adenine (GAA) trinucleotide repeat expansion in the frataxin gene (chromosome 9q21). One untoward effect of frataxin deficiency is lack of iron (Fe)-sulfur clusters, but progressive remodeling of the heart in FA may be more specifically related to sarcoplasmic Fe overload. The Fe-containing inclusions in a small percentage of cardiomyocytes may not represent purely mitochondrial accumulation of the metal. The objective of this work was to re-examine the contribution of Fe to cardiomyocyte hypertrophy, fiber necrosis, and myocardial scarring by a combination of X-ray fluorescence (XRF), slide histochemistry of Fe, and immunohistochemistry of two Fe-related proteins. Polyethyleneglycol (PEG)-embedded human cardiac tissues from left and right ventricular walls; ventricular septum; right atrium; and atrial septum were studied by qualitative and quantitative XRF. Tissues were recovered from the PEG matrix, re-embedded in paraffin, and sectioned for the visualization of Fe, ferritin, and ferroportin. XRF showed quantifiable levels of Fe and zinc (Zn). Regions of significantly increased Fe (1–4 mm^2) were irregularly distributed throughout the working myocardium. Fe granules were sparse in conductive tissue. Zn signals remained unchanged. Robust cytosolic ferritin reaction product occurred in many fibers of the affected regions. Ferroportin displayed no response except in fibers with advanced Fe overload. These observations are at variance with the concept of selective Fe overload only in cardiac mitochondria. Fe-mediated damage to cardiomyocytes and myocardial scarring are more likely due to cytosolic Fe excess.

Keywords

Cardiomyopathy; Ferritin; Ferroportin; Friedreich's ataxia; Iron; X-ray fluorescence

Corresponding author Arnulf H. Koeppen, M.D. Research Service (151) VA Medical Center 113 Holland Ave Albany, N.Y. 12208 USA Tel. 518-626-6377 FAX 518-626-6369 arnulf.koeppen@med.va.gov.

Disclosures The authors declare no conflict of interest.

Introduction

Cardiomyopathy is the leading cause of death in Friedreich's ataxia (FA)[1–4]. Progressive thickening of cardiac walls and declining left ventricular ejection fractions reveal relentless progression and resistance to therapy, and heart disease may antedate neurological manifestations[5]. Campuzano et al[6] identified the mutation in FA as an abnormally long homozygous guanine-adenine-adenine (GAA) trinucleotide repeat expansion in intron 1 of the frataxin gene (chromosome 9q21) that causes a transcriptional block. The authors also recognized the role of frataxin, a mitochondrial protein, in iron (Fe) metabolism. Cardiomyocytes in autopsy[7] and biopsy specimens[5] of FA patients often contain minute Fe-positive inclusions. The clinical cardiological phenotype correlates with the level of the remaining protein, and patients with short GAA repeat expansions and long survival have neither heart disease nor Fe-positive inclusions. Fe accumulation in the hearts of patients with FA does not reach the level of primary or secondary Fe-overload cardiomyopathy[8], and systemic chelation therapy has gained little support. The pathology of the heart in FA has been the subject of many case reports, but sinoatrial node (SAN), atrioventricular node (AVN), and Purkinje fibers have received little attention. In this study, access to 8 whole FA hearts allowed the qualitative and quantitative evaluation of Fe in both working myocardium and cardiac conductive tissues. X-ray fluorescence (XRF) data and matching ferritin immunohistochemistry reported here support the conclusion that FA causes a significant, highly localized, cytosolic increase of cardiac Fe.

Methods

Table 1 lists basic clinical data and heart weights of 8 patients with genetically confirmed FA. Whole hearts were obtained at the time of autopsy through a formal tissue donation program of Friedreich's Ataxia Research Alliance (Downingtown, PA) and National Ataxia Foundation (Minneapolis, MN). Specimens were fixed in 10% neutral buffered formalin. Control specimens (3 men, 5 women, age 41–66 years) were obtained from the National Disease Research Interchange (Philadelphia, PA) and the academic autopsy practice of Albany Medical College (Albany, NY). Mean heart weight (grams ± standard deviation [S.D.]) of the controls was 414 ± 119 (range, 260–541).

The authors received approval from the Institutional Review Board at the Veterans Affairs Medical Center in Albany, NY, for research on tissue samples obtained by autopsy.

Five tissue samples were collected from each heart: left ventricular wall (LVW), right ventricular wall (RVW), ventricular septum (VS), right atrium (RA), and atrial septum (AS). Samples of LVW, RVW, and VS were taken from transverse slices midway between the cardiac apex and atrioventricular groove. RA and AS were dissected according to Aschoff[9] and Anderson et al[10] to obtain SAN and AVN with adjacent working myocardium on the same section.

The preparation of tissue samples and Fe and Zn calibration standards in polyethylene glycol (PEG) for XRF and subsequent tissue recovery were previously described in detail[11]. In brief, cardiac tissues were infiltrated at room temperature by immersion in progressively more concentrated aqueous solutions of polyethylene glycol (PEG 400) (30–90%, weight/vol; Sigma, St. Louis, MO), followed by liquefied PEG 1000 and PEG 1450 at 60°C. After cooling, the solid blocks of PEG 1450 were “faced” by microtome to present a smooth surface for XRF (fig 1). XRF maps were produced by delivery of a monochromatic X-ray beam from a molybdenum target source to the surface of the specimen[12]. The beam moved across a user-defined region of the specimen in a raster-like manner to generate element-specific maps with millimeter scales in the x- and y-axes. The proprietary computer program

(X-Ray Optical Systems, East Greenbush, NY) segmented the maps and assigned pseudocolors to regions of high, low, and intermediate XRF intensity. White and red indicated maximum XRF. Background XRF was obtained from the PEG 1450 matrix outside the limits of the specimen. Calibration standards for the 2 elements in cardiac tissue with highest XRF, Fe and Zn, were prepared from Fe-III- and Zn-II-mesoporphyrin as described before[11]. Ten measurements were made in zones of the tissue samples that exhibited maximum XRF (white or red color). Mean concentrations of these metals in each specimen were obtained by averaging 10 measurements, reducing the values (counts/5 sec) by subtraction of background XRF, and comparing them with the Fe and Zn calibration standards. Results were expressed as μg/ml PEG 1450. Given the high solubility of PEG 1450 in water, the embedded tissues were recovered without distortion and re-embedded in paraffin[11]. Fe and Zn maps were compared with sections stained with hematoxylin and eosin (H&E), and for Fe, cytosolic ferritin, and ferroportin.

Six μm-thick paraffin sections were cut for routine staining with H&E. Trivalent Fe was visualized with Perls's reagents (1% each of potassium ferrocyanide and hydrochloric acid, weight/vol). Paraffin sections were also used for immunohistochemistry with polyclonal anti-human liver holoferritin (2 μg protein/ml; DAKO, Carpinteria, CA) and polyclonal anti-ferroportin peptide (0.21 μg protein/ml). Anti-ferroportin was raised against the antigenic peptide NLHKDTEPKPLEGT linked to keyhole limpet hemocyanin and immuno-affinity-purified under contract with Anaspec (San José, CA). Sections were de-waxed using standard techniques, and endogenous peroxidase activity was suppressed by immersion in methanol containing 3% hydrogen peroxide (30 min). Sections were chelated with a solution of 2,2'-dipyridyl and sodium hydrosulfite solution (2 mM each in acetic acid-sodium acetate buffer, pH 6). Antigen retrieval for ferritin consisted of immersion in DIVA, a proprietary decloaking solution (Biocare Medical, Concord, CA), for 30 min at 95°C. Sections intended for the visualization of ferroportin were heated for 10 min in an autoclave at 120°C while immersed in dilute hydrochloric acid (2 mM). The sequence of incubations following rehydration, oxidation, chelation, and antigen retrieval was: background suppression by normal horse serum (10% by vol) in phosphate-buffered saline (PBS) containing 0.5% bovine serum albumin (BSA; weight/vol) → primary antibody (0.2–4 μg protein/ml in 0.5% BSA in PBS) → secondary biotinylated anti-rabbit IgG (Vector, Burlingame, CA; 0.6 μg protein/ml in PBS) → horseradish peroxidase-labeled streptavidin (2 μg/ml PBS; Sigma, St. Louis, MO) → diaminobenzidine/urea hydrogen peroxide (Sigma).

Fe and Zn levels in regions of maximum XRF were quantified and examined for statistically significant differences (α=0.05) between FA and control samples, using standard t-test.

Results

Mean heart weights of FA patients (Table 1) did not differ significantly from those of 8 normal controls (414±119 g; range 260–541) but were higher than reported for men and women who died from injuries[13]: men, 365±71 (g ± standard deviation [S.D.]; range, 90–630); women, 312±78 (range,174–590). The difference between the control groups is the younger age (men, 42±17 years; women, 49±20 years) and wider weight range in the forensic cases[13]. Heights and weights of the FA patients were not available, and cardiac mass indices could not be calculated.

Figure 1 illustrates PEG 1450-embedded and “faced” gross specimens from the LVW of an FA patient (fig. 1a) and a normal control (Fig. 1d), with matching Fe (figs. 1b and e) and Zn maps (figs. 1c and f). The maps display variation in pseudocolors, indicating the range of XRF signals from high (white and red), to intermediate (orange and green), and low (light and dark blue). All signals have been corrected by subtracting background XRF, rendering

the specimen-free areas of the PEG block black. In the case of FA, the cut surface of a papillary muscle shows the strongest Fe signal (white and red; fig. 1b, circle) while Zn XRF is low (fig. 1c, circle). The control specimen shows heterogeneous Fe (fig. 1e) and Zn signals (fig. 1f). Areas of peak emission for Fe (red, fig. 1e. circle) and Zn (fig. 1f, red) do not coincide.

Table 2 summarizes XRF-based quantitative analyses of Fe and Zn in 5 identified regions of the heart of 8 cases of FA and 8 normal controls. To determine a possible correlation of Fe and Zn, data points on both metals were collected from regions of maximum Fe XRF, such as illustrated by white circles in figs. 1 and 2. All 5 regions of FA myocardium yielded significantly higher Fe concentrations (μg/ml) compared to controls. Mean Zn concentrations in FA hearts did not differ from normal controls. Quantification of Fe and Zn by XRF of PEG 1450-infiltrated tissues was validated by comparison with results obtained by different methods[5,14].

Figure 2 is a systematic display of Fe maps of an FA patient and matching sections stained for Fe, cytosolic ferritin, and ferroportin. The microphotographs were taken from regions with high Fe XRF signals that are circled on the maps of LVW (fig. 2a); RVW (fig. 2b); VS (fig. 2c); RA (fig. 2d); and AS (fig. 2e). Adjacent sections reveal that all cardiomyocytes containing Fe-positive granules are also ferritin-reactive. The immunohistochemical reaction product, however, is not restricted to the granules but fills the entire fiber (figs. 2k–o). Not all ferritin-positive fibers display Fe-positive granules. Figures 2p–t reveal no changes in ferroportin reaction product in fibers that display Fe granules and intense ferritin reaction. Figure 3, however, illustrates a ferroportin response to increasing Fe load. The cardiomyocyte lesion progresses from moderate Fe incorporation (fig. 3a) and diffusely staining cytosolic ferritin (fig. 3d) to even greater Fe accumulation (fig. 3b) and granular ferritin (fig. 3e) and, finally, to replacement of the sarcoplasm by Fe-containing phagocytes (fig. 3c) with complete filling of the fiber by ferritin (fig. 3f). Ferroportin reaction produces changes from diffuse or finely granular (fig. 3g) to coarse granules (fig. 3h, arrow) before it disappears (fig. 3h, star; and 3i). Traces of surface ferroportin immunoreactivity, presumably in macrophages, remain in the necrotic fiber (fig. 3i).

Figure 4 displays adjacent sections of the cardiac conduction system in FA (SAN, AVN, Purkinje fibers). The H&E stain (figs. 4a, d, and g) shows large pale fibers and minor endomysial hypertrophy in SAN (fig. 4a) and AVN (fig. 4d). Fe-positive inclusions are sparse in SAN, AVN, and Purkinje fibers. Ferritin-reactive cardiomyocytes are more abundant in AVN (fig. 4f) than in SAN (fig. 4c) and Purkinje fibers (fig. 4i).

Discussion

FA affects the myocardium of all chambers, but relatively few fibers (1–10%) display Fe-positive inclusions. The XRF maps strongly suggest that subendocardial working myocardium, including papillary muscles (figs. 1b), are more vulnerable than other areas of the LVW, RVW, and VS. The multifocal, rather than diffuse, accumulation of Fe shown by XRF (figs. 1 and 2) explains why chemical assays of Fe in bulk extracts of tissue blocks show no pathological increase in FA patients[5]. The localized Fe accumulation in the hearts of patients with FA differs greatly from the pervasive Fe excess in hemochromatosis[15]. Therefore, inappropriate Fe uptake alone does not explain the pathogenesis of FA cardiomyopathy.

Immunohistochemical visualization of ferritin reaction product is a reliable marker of the Fe status of the affected tissue, and several observations support the interpretation that cardiac Fe excess in FA is mostly *cytosolic* rather than purely *mitochondrial:* (1) Fe-positive

material typically occurs in rows of small blue granules that run parallel to the fibrils of the sarcomere (figs. 2g and j), but ferritin reaction product is not restricted to these granules (figs. 2k–o); (2) histochemical reaction product of mitochondrial ferritin is present in only a small percentage of cardiomyocytes[5]; (3) the relatively large regions on Fe XRF maps (1–4 mm^2) that emit high (white) Fe signals (figs. 2a–e) and the abundant ferritin reaction product in matching sections (fig. 2k–o) are more consistent with Fe in the cytosol rather than in mitochondria; (4) the size of the Fe-positive granules in FA cardiomyocytes (figs. 2f–j) exceeds the dimensions of individual mitochondria. These considerations, however, do not exclude the presence of mitochondrial Fe. Mitochondrial inclusions may become visible at the light level because ferritin-laden organelles occur in rows and clusters, as shown by electron microscopy after bismuth enhancement[4–5].

The vigorous ferritin response exemplified in fig. 3 is most likely due to the interaction of Fe, an iron-regulatory protein (1 or 2), and the iron-regulatory element (IRE) in the 5'-untranslated region (5'-UTR) of ferritin messenger ribonucleic acid (mRNA). Though ferroportin mRNA also contains an IRE in its 5'-UTR, this cardiac protein does not appear to respond to the cytosolic Fe accumulation (fig. 2) until a more advanced stage of fiber destruction (fig. 3). Aggregation and ultimate disappearance of ferroportin immunoreactivity (figs. 3h and i) that accompany increased expression of ferritin (figs. 3e and f) may represent hepcidin-induced protein ubiquitination and proteolytic digestion[16].

The interpretation of data presented here may benefit from detailed studies of Fe-related proteins in the muscle creatinine kinase (MCK) mouse model with targeted frataxin deficiency in cardiac and skeletal muscle[17–19]. The phenotype of the MCK conditional frataxin knockout mouse[17] strongly resembles the cardiac pathology of FA in humans. The systematic analysis of Fe-related proteins led authors[18–19] to believe that Fe accumulation in FA heart is *mitochondrial* and occurs at the expense of cytosolic Fe. These conclusions are difficult to reconcile with the findings in human FA cardiomyopathy in which cytosolic ferritin increases (figs. 2 and 3). It is possible that human FA and its MCK mouse equivalent share cytosolic Fe deficiency at an early stage of cardiomyopathy due to increased avidity of mitochondria for this metal. The human heart, however, appears to overcome the hypothesized cytosolic Fe deficit through up-regulation of Fe import. The inappropriate increase of cytosolic Fe stimulates ferritin mRNA translation, and aggregation of ferritin leads to the formation of histochemically reactive Fe granules of varying size.

The density of Fe-containing cardiomyocytes does not correlate with the local severity of the cardiac lesion. In some cases, sections of LVW and VS disclose extensive scarring and loss of contractile fibers that may reach 50% of the cross-sectional area. Fe-containing cardiomyocytes are often located at the junction between fields of severe endomysial hypertrophy and better preserved heart tissue. In the working myocardium of RVW, RA, and AS, Fe-containing fibers are as frequent as in LVW and VS but endomysial connective tissue is less prominent. In contrast to working myocardium, however, SAN, AVN, and the Purkinje bundle contain very few fibers with Fe-positive granules (fig. 4). Conductive tissue also shows minimal if any fibrosis (fig. 4). The sparse Fe load in conductive fibers may be why bradyarrhythmia or tachyarrhythmia generated in the diseased myocardium are relatively infrequent causes of death in FA compared congestive heart failure[20].

Frataxin has multiple functions, and deficiency of the protein exacts complex damaging effects on tissues[4]. Lack of Fe-sulfur clusters impairs the proper operation of mitochondrial complexes I, II, and III, aconitase, and ferrochelatase. Beyond insufficient synthesis of high-energy phosphates, frataxin deficiency is thought to cause Fe-mediated oxidative damage to vulnerable tissues. Bayot et al[21], however, considered Fe accumulation in FA an irrelevant epiphenomenon while accepting a primarily mitochondrial localization of the metal. In

contrast, we propose that the pathogenesis includes accelerated uptake of Fe into cardiomyocytes; enhanced translation of cytosolic ferritin mRNA; aggregation of ferritin; release of ionic Fe from ferritin granules; Fe-mediated oxidative damage to cardiac myofibrils; rupture of cardiomyocytes primarily in working myocardium; phagocytosis and removal of Fe-rich cellular debris; and replacement of necrotic fibers by scar tissue. The process continues in neighboring fibers subject to excessive Fe uptake until a critical number of cardiomyocytes has been destroyed. Wall stress may contribute to the greater vulnerability of the LVW and VS to Fe accumulation and fiber destruction (figs. 2a and c) but is probably insufficient to explain the differential susceptibility of the myocardium and the seeming exemption of the conductive system. Also, many unanswered questions remain about the non-uniform cardiac Fe accumulation in FA.

Rupture of Fe-laden mitochondria is an unlikely source of cytosolic Fe excess, and the study of FA cardiomyopathy must consider direct uptake of the metal into the cytosol from the circulating blood. The interaction of transferrin and transferrin receptor(s) is thought to be less important in heart than transfer through L-type voltage-dependent calcium channels (LVDCC) and the operation of the divalent metal transporter 1[22]. Fe-mediated oxidative damage may not be the only mechanism underlying cardiomyocyte necrosis. The main problem in FA remains deficiency of mitochondrial frataxin, and cardiomyocytes may become vulnerable by mechanisms not directly related to Fe. In support of apoptosis, caspase-3 immunostaining shows an excess of immunoreactive cardiomyocytes in the MCK mouse[23].

The present observations made on FA hearts do not provide insight into the potential value of chelation. If cytosolic Fe deficiency is indeed a critical step in the pathogenesis of FA cardiomyopathy, removal of Fe by a systemic chelating agent might be detrimental. If LVDCC are substantially involved in the Fe overload of FA, calcium channel blockers may be beneficial, as proposed by Oudit et al[22] for primary and secondary cardiac hemochromatosis.

It is unknown whether Zn, alone or in combination with Fe, is relevant to the pathogenesis of FA cardiomyopathy. Though Zn levels are stable throughout the heart in FA (Table 2), the metal may augment oxidative damage in the presence of elevated Fe. A similar mechanism involving 2 transition metals, namely, Fe and Cu, may exist in the pathogenesis of the cerebellar lesion in FA[11].

Acknowledgments

The authors express their gratitude to the families of FA patients who donated tissues for research. Seven of the eight normal hearts were provided by National Disease Research Interchange with support from National Institute of Health grant 5 U42 RR006042. This work was completed in the research laboratories of the Veterans Affairs Medical Center, Albany, N.Y. Dr. Mohammad El-Hajjar critically reviewed the manuscript and assisted the authors in their discussion of clinicoanatomic correlation.

This work was supported by Friedreich's Ataxia Research Alliance, Downingtown, PA; National Ataxia Foundation, Minneapolis, MN; National Institutes of Health (R01 NS069454), Bethesda, MD; and Neurochemical Research, Inc., Glenmont, N.Y.

References

1. Andermann E, Remillard GM, Goyer C, Blitzer L, Andermann F, Barbeau A. Genetic and family studies in Friedreich's ataxia. Can J Neurol Sci. 1976; 3:287–301. [PubMed: 1000412]
2. Harding AE, Hewer L. The heart in Friedreich's ataxia: a clinical and electrocardiographic study of 115 patients, with an analysis of serial electrocardiographic changes in 30 cases. Q J Med NS. 1983; 52:489–502.

3. Dürr A, Cossée M, Agid Y, Campuzano V, Mignard C, Penet C, Mandel JL, Brice A, Koenig M. Clinical and genetic abnormalities in patients with Friedreich's ataxia. N Engl J Med. 1996; 335:1169–1175. [PubMed: 8815938]
4. Koeppen AH. Friedreich's ataxia: Pathology, pathogenesis, and molecular genetics. J Neurol Sci. 2011; 303:1–12. [PubMed: 21315377]
5. Michael S, Petrocine SV, Qian J, Lamarche JB, Knutson MD, Garrick MD, Koeppen AH. Iron and iron-responsive proteins in the cardiomyopathy of Friedreich's ataxia. Cerebellum. 2006; 5:257–267. [PubMed: 17134988]
6. Campuzano V, Montermini L, Moltò MD, Pianese L, Cossée M, Cavalcanti F, Monros E, Rodius F, Duclos F, Monticelli A, Zara F, Cañizares J, Koutnikova H, Bidichandani SI, Gellera C, Brice A, Trouillas P, De Michele G, Filla A, De Frutos R, Palau F, Patel PI, Di Donato S, Mandel JL, Cocozza S, Koenig M, Pandolfo M. Friedreich's ataxia: autosomal recessive disease caused by an intronic GAA triplet repeat expansion. Science. 1996; 271:1423–1427. [PubMed: 8596916]
7. Lamarche JB, Côté M, Lemieux B. The cardiomyopathy of Friedreich's ataxia. Morphological observations in 3 cases. Can J Neurol Sci. 1980; 7:389–396. [PubMed: 6452194]
8. Murphy CJ, Oudit GY. Iron-overload cardiomyopathy: Pathophysiology, diagnosis, and treatment. J Cardiac Fail. 2010; 16:888–900.
9. Aschoff L. Referat über die Herzstörungen in ihren Beziehungen zu den spezifischen Muskelsystemen des Herzens. Verhandl Deutsch Pathol Gesellsch. 1910; 14:3–35.
10. Anderson RH, Yanni J, Boyett MR, Chandler NJ, Dobrzynski H. The anatomy of the cardiac conduction system. Clin Anat. 2009; 22:99–113. [PubMed: 18773472]
11. Koeppen AH, Ramirez RL, Yu D, Collins SE, Qian J, Parsons PJ, Yang KX, Chen Z, Mazurkiewicz JE, Feustel PJ. Friedreich's ataxia causes redistribution of iron, copper, and zinc in the dentate nucleus. Cerebellum. 2012 doi: 10.1007/s12311-012-0383-5.
12. Chen ZW, Gibson WM, Huang H. High-definition X-ray fluorescence: principles and techniques. X-Ray Opt Instrum. 2008 doi:10.1155/2008/318171.
13. De la Grandmaison GL, Clairand I, Durigon M. Organ weight in 684 adult autopsies: new tables for a Caucasoid population. For Sci Int. 2001; 119:149–154.
14. Rahil-Khazen R, Bolann BJ, Myking A, Ulvik RJ. Multi-element analysis of trace element levels in human autopsy tissues by using inductively coupled atomic emission spectrometry technique (ICP-AES). J Trace Elem Med Biol. 2002; 16:15–25. [PubMed: 11878748]
15. Keschner HW. The heart in hemochromatosis. South Med J. 1951; 44:927–931. [PubMed: 14876519]
16. Qiao B, Sugianto P, Fung E, Del Castillo-Rueda A, Moran-Jimenez M-J, Ganz T, Nemeth E. Hepcidin-induced endocytosis of ferroportin is dependent on ferroportin ubiquitination. Cell Metab. 2012; 15:918–924. [PubMed: 22682227]
17. Puccio H, Simon D, Cossée M, Criqui-Filipe P, Tiziano F, Melki J, Hindelang C, Matyas R, Rustin P, Koenig M. Mouse models for Friedreich ataxia exhibit cardiomyopathy, sensory nerve defect and Fe-S enzyme deficiency followed by intramitochondrial iron deposits. Nat Genet. 2001; 27:181–186. [PubMed: 11175786]
18. Huang ML, Becker EM, Whitnall M, Rahmanto YS, Ponka P. Elucidation of the mechanism of mitochondrial iron loading in Friedreich's ataxia by analysis of a mouse mutant. Proc Natl Acad Sci USA. 2009; 106:16381–16386. [PubMed: 19805308]
19. Whitnall M, Rahmato YS, Sutak R, Xu X, Becker EM, Mikhael MR, Ponka P, Richardson DR. The MCK mouse heart model of Friedreich's ataxia: Alterations in iron-regulated proteins and cardiac hypertrophy are limited by iron chelation. Proc Natl Acad Sci USA. 2008; 105:9757–9762. [PubMed: 18621680]
20. Tsou AY, Paulsen E, Lagedrost SJ, Perlman SL, Mathews KD, Wilmot GR, Ravina B, Koeppen AH, Lynch DR. Mortality in Friedreich's ataxia. J Neurol Sci. 2011; 307:46–49. [PubMed: 21652007]
21. Bayot A, Santos R, Camadro J-M, Rustin P. Friedreich's ataxia: the vicious circle hypothesis revisited. BMC Medicine. 2011; 9:112. [PubMed: 21985033]
22. Oudit Y, Sun H, Trivieri MG, Koch SE, Dawood F, Ackerley C, Yazdanpanah M, Wilson GJ, Schwartz A, Liu PP, Backx PH. L-type Ca^{2+} channels provide a major pathway for iron entry into

cardiomyocytes in iron-overload cardiomyopathy. Nat Med. 2003; 9:1187–1194. [PubMed: 12937413]

23. Payne RM, Pride PM, Babbey CM. Cardiomyopathy of Friedreich's ataxia: Use of mouse models to understand human disease and guide therapeutic development. Pediatr Cardiol. 2011; 32:366–378. [PubMed: 21360265]

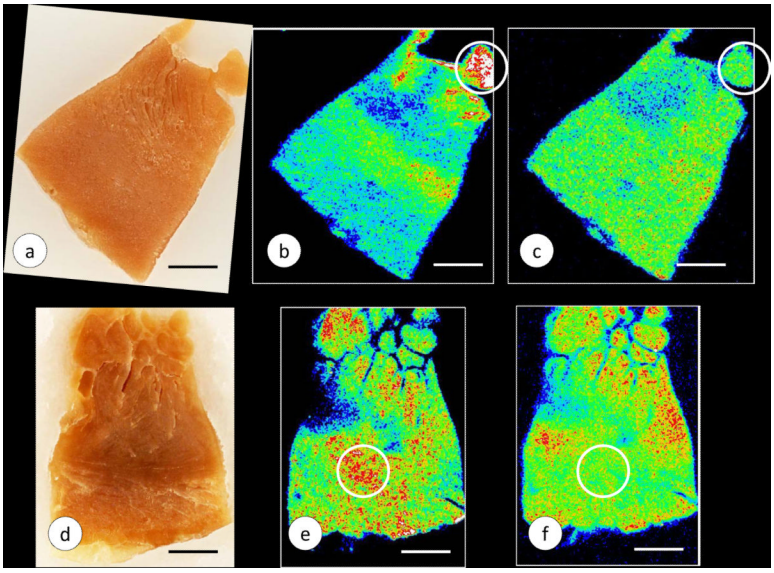

Figure 1.

Alignment of Fe and Zn XRF arising from PEG-embedded samples of myocardium. (a)–(c), FA; (d)–(f) control. (a) and (d), PEG 1450 block containing heart tissue from the LVW; (b) and (e) Fe XRF; (c) and (f) Zn XRF. The Fe signal of the FA heart shows a somewhat irregular distribution with peak XRF arising from a papillary muscle (circle in b). The same region (c, circle) shows a low Zn signal. The distribution of Zn in the LVW of FA (c) is more homogeneous than that of Fe. The circles in (e) and (f) show an example of regional comparison of Fe and Zn concentrations. Bars, 5 mm.

Abbrev.: FA, Friedreich's ataxia; Fe, iron; LVW, left ventricular wall; PEG, polyethyleneglycol; XRF, X-ray fluorescence; Zn, zinc

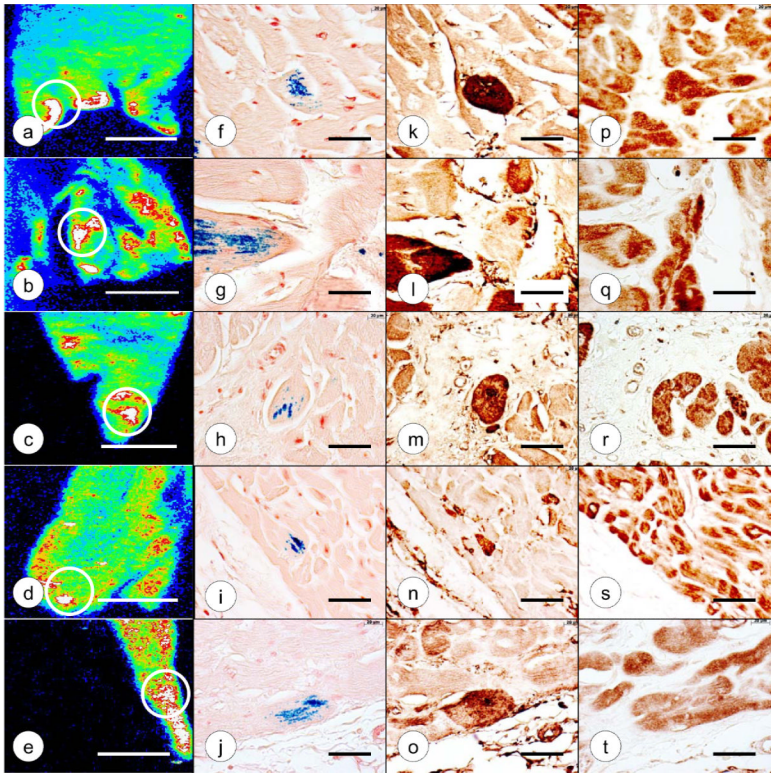

Figure 2.

Comparison of Fe XRF maps, Fe histochemistry, ferritin and ferroportin immunohistochemistry in FA. (a)–(e), Fe XRF; (f)–(j), Fe histochemistry (brazilin counterstain); (k)–(o), ferritin immunohistochemistry; (p)–(t), ferroportin immunohistochemistry. From top to bottom, the cardiac tissues are: LVW (a, f, k, p); RVW (b, g, l, q); VS (c, h, m, r); RA (working myocardium) (d, i, n, s); AS (working myocardium) (e, j, o, t). The contiguous microphotographs correspond to the circled region on the XRF maps. All cardiomyocytes with blue Fe reaction product display abundant immunohistochemical reaction product of ferritin. Not all ferritin-positive fibers show histochemical reaction product of Fe. Ferroportin reaction product is abundant in all samples of myocardium and does not seem to change in step with the accumulation of Fe or ferritin (however, see fig. 3). Bars in Fe XRF maps, 5 mm; all other bars, 50 μm. Abbrev.: AS, atrial septum; FA, Friedreich's ataxia; Fe, iron; LVW, left ventricular wall; RA, right atrium; RVW, right ventricular wall; VS, ventricular septum; XRF, X-ray fluorescence.

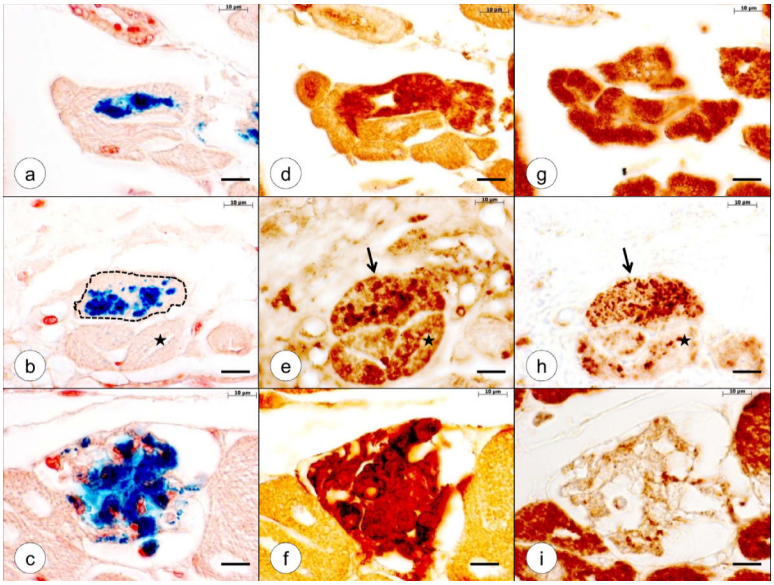

Figure 3.

Progressive destruction of cardiomyocytes in FA (patient 2, Table 1). (a)–(c), Fe histochemistry (brazilin counterstain); (d)–(f), ferritin immunohistochemistry; (g)–(i), ferroportin immunohistochemistry. The staining of adjacent sections for Fe, ferritin, and ferroportin illustrates progressive cardiomyocyte lesions. In the top panel, the cardiomyocyte (a) is still intact, but ferritin reaction product is present throughout the entire sarcoplasm (d). In this fiber, ferroportin reaction product shows no difference from the adjacent low-ferritin fibers. The middle panel illustrates a more seriously affected cardiomyocyte. Fe fills most of the sarcoplasm of the fiber (b; outlined by an interrupted line). Ferritin reaction product in the same fiber is granular rather than diffuse (e; arrow). Ferroportin also appears clumped (h, arrow). The fiber marked by stars (b, e, h) displays only minimal Fe reaction product (b) but strong granular ferritin immunoreactivity (e). Ferroportin in this fiber appears depleted (h). The bottom panel shows end-stage fiber destruction (c, f, i). Fe reaction product is present in coarse clumps representing phagocytized metal (c). Ferritin reaction product completely fills the gutted fiber (f). Only traces of ferroportin reaction product, presumably in macrophages, remain (i). Bars, 10 μm (oil immersion). Abbrev.: FA, Friedreich's ataxia; Fe, iron

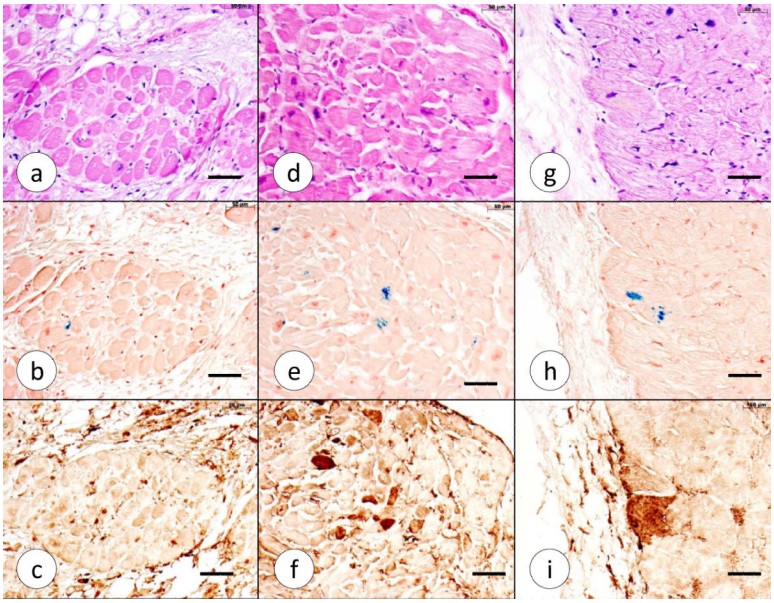

Figure 4.

Fe and ferritin in the cardiac conduction system in FA. (a)–(c) SAN, (d)–(f) AVN, (g)–(i) Purkinje fibers of the VS (a–f, case 1, Table 1; g–i, case 6, Table 1). Contiguous sections were stained with H&E (a, d, g); for Fe (b, e, h); and ferritin (c, f, i). Compared with working myocardium (see figs. 1 and 2), Fe deposits in conductive fibers are infrequent. Ferritin reaction product is present in cardiac conduction fibers and the endomysium of SAN and AVN, and endothelial cells covering Purkinje fibers (c, f, and i, respectively). Bars, 50 μm. Abbrev.: AVN, atrioventricular node; FA, Friedreich's ataxia; Fe, iron; H&E, hematoxylin and eosin; SAN, sinoatrial node; VS, ventricular septum

Am J Cardiol. Author manuscript; available in PMC 2013 December 15.

Table 1

Basic clinical information on 8 patients with Friedreich's ataxia

Patient	Sex	Age at onset (years)	Age at death (years)	Disease duration (years)	GAA repeats		Heart weight (g)
					Allele 1	Allele 2	
1	M	7	34	27	1114	1114	418
2	M	8	27	19	1070	700	413
3	F	8	23	15	864	668	358
4	M	9	33	24	925	925	421
5	M	10	24	14	1050	700	547
6	F	10	24	14	910	740	427
7	F	15	69	54	560	560	359
8	F	20	50	30	1122	515	487
Mean ± S.D.		11 ± 4	36 ± 16	25 ± 13	952 ± 186	740 ± 195	429 ± 63

Abbrev.: FA, Friedreich's ataxia; S.D., standard deviation

Table 2

Iron and zinc levels in 5 regions of myocardium in Friedreich's ataxia and controls; and statistical comparison

Fe	***n***	**LVW**	**RVW**	**VS**	**RA**	**AS**
FA	8	190.8 ± 58.1	113.2 ± 43.8	180.4 ± 75.4	114.5 ± 43.2	98.4 ± 33
Controls	8	115.2 ± 25.5	73.5 ± 26.3	96.6 ± 25.5	54.7 ± 22.7	60.0 ± 17.1
p-value		***0.005***	***0.045***	***0.012***	***0.004***	***0.016***
Zn						
FA	8	24.1 ± 11.2	21.5 ± 16.7	29.8 ± 21.5	14.3 ± 7	15.1 ± 6.7
Controls	8	26.2 ± 6.5	20.0 ± 6.7	28.6 ± 10.6	13.7 ± 8.9	15.9 ± 13.1
p-value		***0.64***	***0.811***	***0.886***	***0.878***	***0.88***

Values for Fe and Zn levels are the group means (μ/ml) ± standard deviations.

Abbrev.: AS, atrial septum; FA, Friedreich's ataxia; Fe, iron; LVW, left ventricular wall; RA, right atrium; RVW, right ventricular wall; VS, ventricular septum; Zn, zinc.